Response to Reviewer #1's Comments:

Jiayi Li et al. (Author)

We would like to express our sincere gratitude to Reviewer #1 for the insightful and professional comments. We provide the following response to Reviewer #1's comments regarding the data and methods. Overall, the changes to the methods do not significantly affect our final results if we do not use r_e < 14 μm as suggested. The revised results is attached at the end of the response for reviewer's reference.

Specific Responses:

1. The retrievals of cloud properties:

The native resolution of the AHI is 2 km. Why use a microphysical product of 4 km? The low resolution renders the retrieval very sensitive to errors due to partial pixel feeling in most cases, except for the fully cloudy scenes. Therefore, the effects of cloud cover are confounded with those on LWP.

Response: Thanks for your great comment. Although the native resolution of AHI is higher, the official AHI dataset only provides the effective radius (r_e) Level-2 product for the 2.3 μm channel. In contrast, the SatCOPRS CERES Geostationary Satellite Edition 4 Himawari-8 product we used (CER_GEO_ED4_HIM08_NH_V01.2, CER_GEO_ED4_HIM08_SH_V01.2) has a coarser resolution but provides r_e Level-2 product for the 3.9 μm channel using the Langley Research Center (LARC)s SatCORPS algorithms in support of CERES project. This product with the 3.9 μm channel is considered more accurate for cloud droplet number concentration (N_d) retrievals because this channel better represents the cloud-top information, introducing less bias to the retrieval of N_d (25%~38% for 2.3μm, less than 20% for 3.7 μm according to Grosvenor et al., 2018).

Additionally, the 3.9 μm r_e from CER_GEO_ED4_HIM08 shows good consistency with the 3.7 μm r_e from MODIS (Figure R1), supporting us in obtaining more accurate N_d. While the coarser resolution may impact the retrieval to some extent as the reviewer said, SatCOPRS CERES Geostationary Satellite cloud product only uses cloudy pixels based on the CERES Ed4 cloud mask (Trepte et al., 2019; Yost et al., 2021), thus largely avoiding the situation mentioned by the reviewer.

Considering the overall quality of the product and the existing precedent of using SatCOPRS CERES Geostationary Satellite products in studies for LWP adjustments (Qiu et al., 2024), we finally selected this dataset in our study.

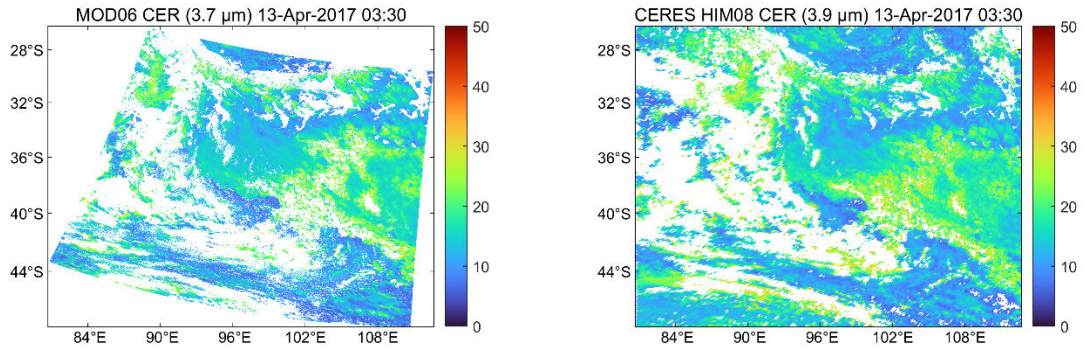

Figure R1. Comparison of the 3.7 μm r_e from MODIS and the 3.9 μm r_e from CER_GEO_ED4_HIM08_SH_V01.2.

Why sub-sampling the data? Why is it 8 km at the NH and 6 km at the SH?

Response: Thank you for raising this question. The description of the data resolution in the manuscript was based on the data introduction available on the NASA EARTHDATA SEARCH (https://search.earthdata.nasa.gov/search/granules/collection-details?p=C1584977037-LARC_ASDC&pg[0][v]=f&pg[0][gsk]=-start_date&fpj=CERES&lat=0.0703125&long=-0.0703125). However, after reaching out to technical staff through the Earthdata forum for clarification, we learned that the information on the website is incorrect. The observation resolution of CERES_GOES_HIM08 is 2 km at nadir, and has been sub-sampled to 6 km for both the Northern and Southern Hemispheres. The sub-sampled resolution meets the needs of the CERES project without having a data implosion.

We provide the link to our post and the related response from the technical staff for the reviewer's reference (https://forum.earthdata.nasa.gov/viewtopic.php?t=6315). We have corrected this issue in the revised version of the manuscript.

2. There is no justification for the threshold of r_e < 14 μm. While larger r_e allows more water loss by precipitation, it may be more than balanced by less water loss due to less evaporation of the larger cloud drops.

3. Furthermore, r_e increases with cloud geometrical depth (CGT) and LWP increases with CGT^2. Therefore, excluding scenes by their r_e values is incurring bias, rendering the whole study questionable

4. Line 131: The positive trend of LWP with N_d was previously documented to occur only at N_d<30 cm^{-3} (Figure 2 of Gyspeerdt et al., 2019). The clouds have to be very shallow with respectively small LWP for r_e<14 in clouds with N_d<30 cm^{-3}.

In fact, the condition of r_e<14 um imposes an artifact of more LWP with larger N_d, because with larger N_d the cloud needs to grow deeper and have larger LWP for reaching r_e=14 µm at the cloud top !!!

1. Indeed, this study's maximum LWP is shifted from 30 (Figure 2 of Gyspeerdt et al., 2019) to nearly 100 cm^{-3}. This is evident in Fig1 left panels, especially in the convective regime (AUW), where cloud thickness and, hence, LWP consistently increase with N_d. This artifact dominates the results of this study.

Response: We agree with this great point, and we sincerely appreciate the reviewer's professional comments. Since these comments all relate to the threshold of r_e < 14 µm, we will address this point below.

This issue was discussed earlier in the study. The reason for choosing the threshold of r_e < 14 µm is that the invalidation of adiabatic assumptions for N_d retrievals under precipitation conditions can introduce bias. For example, Grosvenor et al. (2018) suggests in their review paper on N_d retrieval that "As a precautionary measure, it may be prudent to attempt to filter out situations with precipitation before performing N_d retrievals". Kang et al. (2021), using aircraft observations, also pointed out that removing precipitation enhances the retrieval accuracy of r_e in SatCORPS Himawari-8 product, which is an important variable affecting N_d retrieval. Therefore, in order to obtain more accurate N_d values and focus on the microphysical processes within non-precipitating clouds, we firstly used GPM IMERG hourly precipitation product to exclude precipitation scenes. However, considering GPM's limited ability to detect light drizzle, we additionally applied r_e < 14 µm threshold based on suggestions according to Rosenfeld et al. (2012), which has been widely used to distinguish between precipitating and non-precipitating clouds (Possner et al., 2020; Rosenfeld et al., 2019).

We acknowledge the reviewer's concern on using the threshold of r_e < 14 µm. The sensitivity analysis on whether to exclude precipitation has been conducted. Figure R2 shows the N_d-LWP relationship and the diurnal variations LWP adjustments under different precipitation criteria. In both regions, the threshold application primarily removes cloud samples with small N_d and large LWP, located in the upper left of the N_d-LWP space. Specifically, in AUW region, the diurnal pattern shows little change before noon, and without the threshold of r_e <14 µm, the afternoon variation becomes smaller, indicating that the samples we excluded primarily affected the afternoon results. This may be because clouds with larger r_e and larger LWP primarily occur in the afternoon. In the morning, r_e is relatively small, so adding the threshold of r_e < 14 µm does not significantly affect the dominant samples. However, in the afternoon,

as r_e increases, the inclusion of samples with smaller N_d and larger LWP causes the LWP adjustments to become more negative. The results using only GPM criterion are similar to those without any precipitation restriction, indicating the diurnal pattern is dominated by non-precipitating samples. In the ECS region, adding the threshold of r_e < 14 μm has little impact on the diurnal pattern of LWP adjustments, mainly affecting the values. This is likely because the ECS region is characterized by smaller r_e values with heavily influence by anthropogenic aerosol pollution. Most precipitation samples are excluded by GPM.

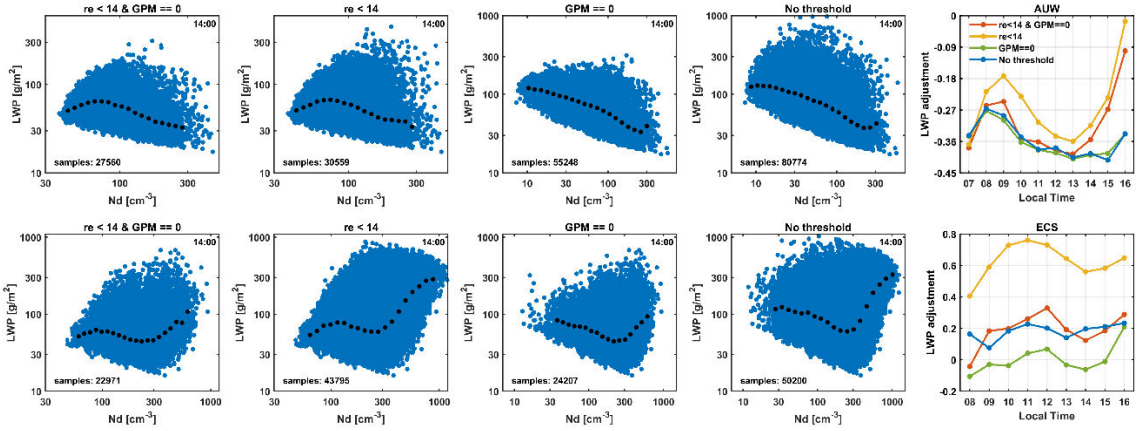

Figure R2. Comparison of the N_d-LWP relationship and diurnal variations of LWP adjustments under different precipitation screening criteria in two typical regions (the west of Australia, AUW) and the east China sea, ECS). Blue dots are all sample within the N_d-LWP space at 1400 LT. Black dots represent median LWP in each N_d bin.

Based on the results of the above sensitivity analysis, and considering the aim to minimize the significant uncertainties that heavy precipitation may introduce to the retrieval of N_d. We have decided not to use the r_e < 14 μm threshold following the reviewer's suggestion, but we still retain the exclusion of heavy precipitation scenes with the criteria of GPM = 0.

Adjusting the precipitation criteria means that we need to revise the results of the manuscript. Overall, the diurnal variations of other cloud properties in the revised results section have not changed significantly and the conclusions of our paper and the underlying physical processes remain unaffected. The changes include the values of LWP adjustments and their impact on aerosol indirect effects. We have highlighted the revised sections in red color which are provided below for the reviewer's reference.

3 Results

3.1 LWP adjustments vary alongside microphysical-dynamical conditions

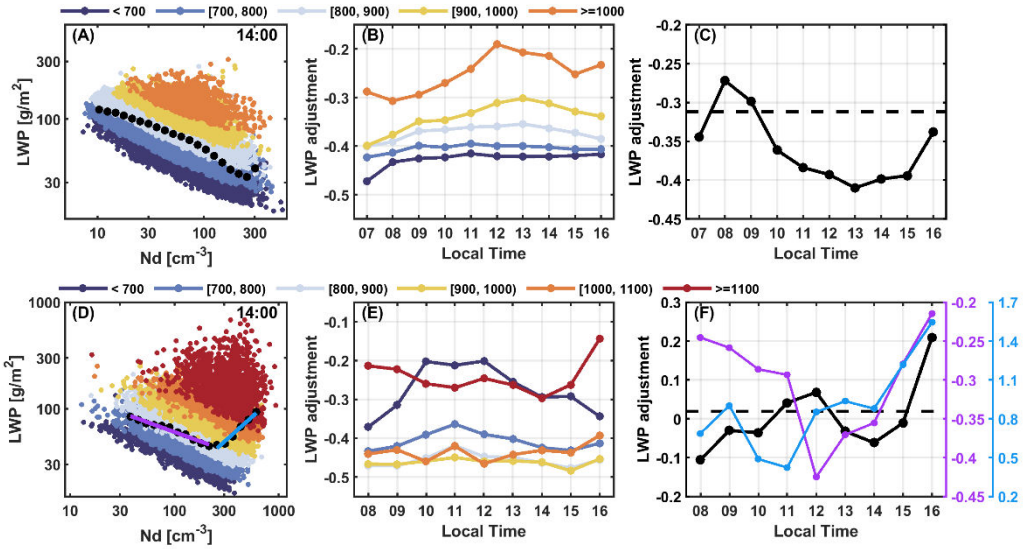

Figure 1. LWP adjustments in log-log spaces and their diurnal patterns in two typical regions (the west of Australia, AUW) and the east China sea, ECS). Non-precipitation cloud samples scattered in N_d-LWP log space at 1400 LT in (A) AUW and (D) ECS region. Colored dots are samples in different cloud thickness (H) bins (unit: m). Black dots represent median LWP in each N_d bin. The colored lines are the fits of black dots at different stages in ECS region. Diurnal variations of LWP adjustments binned by H in (B) AUW and (E) ECS region are showed. Colored lines in (F) are diurnal variations of different stages in (D), while black lines in (C) and (F) are the overall diurnal variations of LWP adjustments in two regions, respectively. Dashed lines represent the average LWP adjustments considering diurnal variations, –0.31 for AUW (C) and 0.02 for ECS (F).

Figure 1 (A and D) shows the scatter plots of N_d-LWP relationship in log-log space for AUW and ECS regions at 1400 LT (local time), respectively. The complete pictures of all available daytime periods are presented in Figure S2. N_d-LWP relationships show similar patterns during daytime in each region but different results in two regions, with an overall negative adjustment in AUW, meaning that LWP decreases with increased N_d, while the LWP adjustments in ECS region exhibit both positive and negative throughout the day. For non-precipitation clouds, both positive and negative LWP adjustments have been reported (Glassmeier et al., 2021; Michibata et al., 2016; Rosenfeld et al., 2019; Toll et al., 2019), caused by different mechanisms (e.g. lifetime effect and entrainment feedbacks) (Michibata et al., 2016). In fact, conflicting LWP adjustments are ultimately subject to the dominant microphysical-dynamical

mechanisms for each N_d stage. Before 300 cm^{-3}, LWP adjustments are dominated by processes at the cloud margins, such as sedimentation-entrainment feedbacks and evaporation-entrainment feedbacks (Ackerman et al., 2004; Small et al., 2009), leading to negative LWP adjustments in both regions (Figure 1A and purple line in Figure 1D).

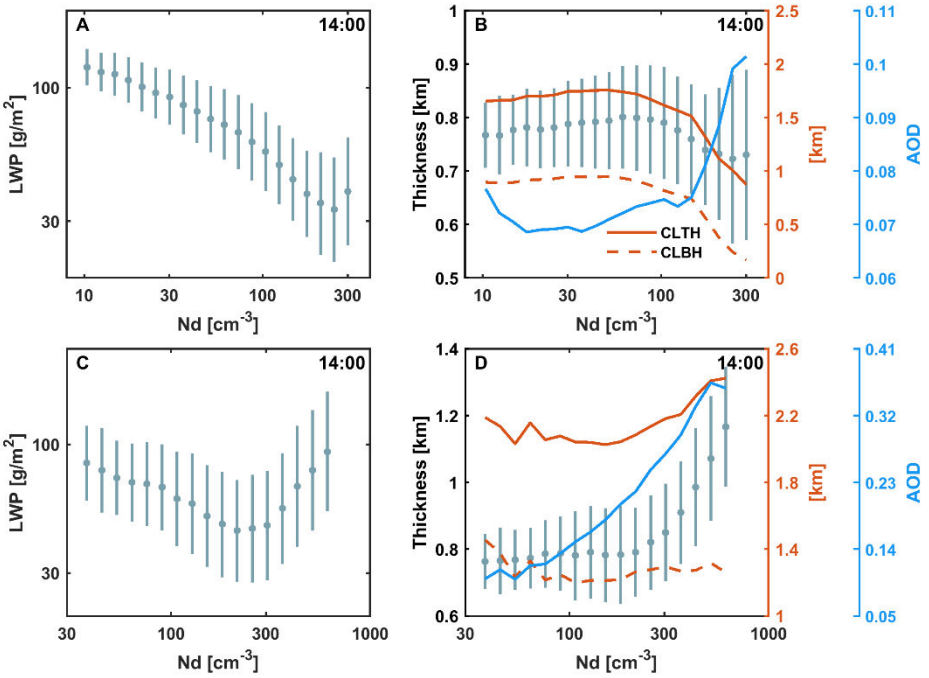

Figure 2. Comparisons between N_d-LWP relationship and N_d-Thickness relationship in two regions. Relationship between N_d and (A) LWP, (B) cloud thickness in AUW region. Relationship between N_d and (C) LWP, (D) cloud thickness in ECS region. The orange solid and dashed lines show the change of cloud top height (CLTH) and cloud bottom height (CLBH) with N_d.

However, LWP begins to rise at high N_d in ECS (blue line in Figure 1D), which is the primary reason causing the overall positive LWP adjustments in this region. Positive sensitivity over ECS has been reported but not fully understood (Bender et al., 2019; Gryspeerdt et al., 2019; Michibata et al., 2016; Zhang et al., 2021). Michibata et al. (2016) attributed the positive LWP response in non-precipitation clouds over East Asia to cloud lifetime effect. Gryspeerdt et al. (2019) reported the rising behavior at high N_d, especially at moist conditions, however, their samples ended around 300 cm^{-3}. Here in ECS region, clouds are heavily affected by anthropogenic aerosols, showing LWP increases with N_d at high N_d (>300 cm^{-3}). The increasing of LWP at high N_d seems to indicate the increasing N_d provides a larger surface area for condensation and finally compensating the effect of entrainment (Lee et al., 2009). Furthermore, we found this behavior is consistent with deepening of cloud depth (Figure 2, C and D)

which is likely induced by the latent heat released by condensation, indicating the invigoration effect by aerosols (Altaratz et al., 2014). To exclude the influence of Simpson's Paradox (thicker cloud samples along the coast with larger N_d and thinner ones with smaller N_d offshore), we divide the samples into coastal and offshore groups and found that the observed pattern is not significantly affected by the geographical region (Figure S3).

Although the microphysical-dynamical processes are challenging to be observed directly, environmental conditions can be considered as proxy and provide further support for invigoration effect. Cloud droplets are more likely to grow in the unstable and moist atmosphere in ECS, with a mean lower-tropospheric stability (LTS) of 15.94 K and a peak in relative humidity on 700 hPa (RH700) of 70% (Figure 3). Additionally, according to the division from Rosenfeld et al. (2019), we categorize the clouds into Sc (LTS > 18 K), Sc to Cu transition (14 K ≤ LTS ≤ 18 K) and Cu (LTS < 14 K) (Figure 4, G, H and I). Clouds in ECS region are dominated by the Sc to Cu transition regime.

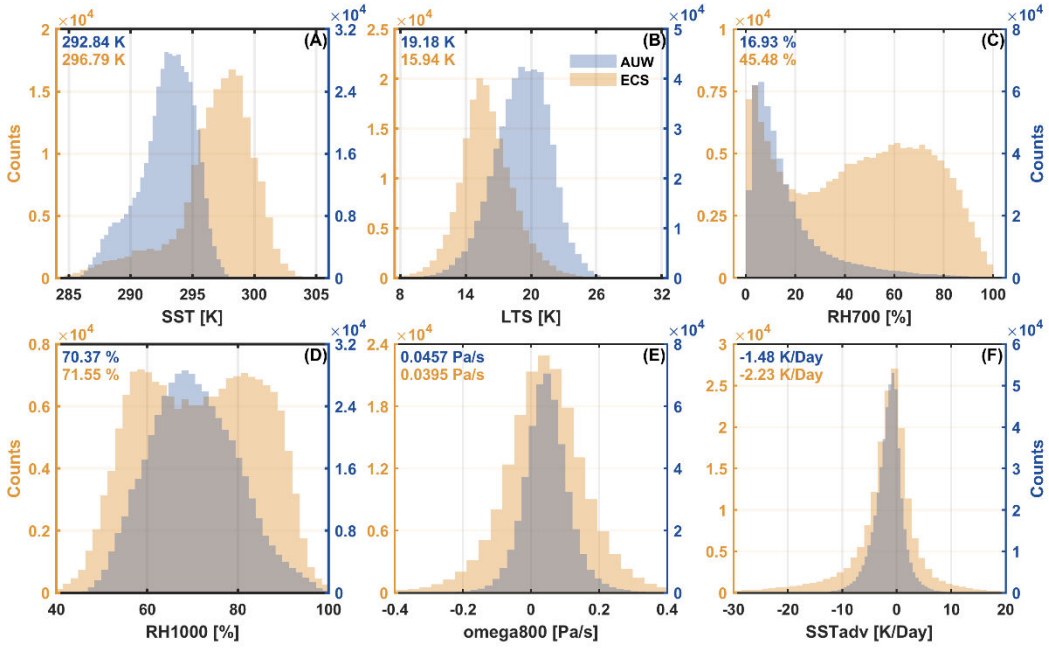

Figure 3. 4-year meteorological conditions of non-precipitation clouds in AUW and ECS region from 2016 to 2019. Histograms of meteorological factors are presented here. The mean values are labeled in the top-left corner. Data are directly or indirectly derived from ERA5. For vertical velocities on 800 hPa (omega800), positive (negative) values indicate downdraft (updraft).

The formation of this transition regime is associated with increasing sea surface temperature (SST) due to "deepening-warming decoupling" (Albrecht et al., 1995; Bretherton and Wyant, 1997). Sc presents over the relatively shallow and stable boundary layer with cooler sea surface along the coast (Figure 4,

A and B) and most of Sc may be mainly advected from the southeast Chinese plain (Klein and Hartmann, 1993). According to the cloud advection scheme by Miller et al. (2018), cloud advection can be approximated as the translation of the cloud field with the wind field. The advection height assumed to correspond to the height of the cloud top. Therefore, we can simply deduce from the wind field at 700 hPa that clouds in ECS have the possibility of advection from the Chinese plain in the west (Figure S4). As air moves offshore, MBL deepens and cloud layer decouples with the surface mixed layer over warmer sea surface. Cu forms in the moist and unstable subcloud layer and rises to upper cloud layer, resulting in a local cumulus-coupled MBL. Warm invigoration, in which aerosols promote water vapor condensation by acting as CCN, releasing latent heat and promoting cloud vertical development, mainly occurs in these convective clouds, consistent with Zhang et al. (2021). They also attributed the positive LWP adjustments in ECS to warm invigoration with the low-level convective clouds (Sc and Cu) domain by MODIS and CloudSat measurements. Kaufman et al. (2005) also reported larger LWP in higher aerosol loading conditions over Atlantic in warm clouds (a mix of stratus and trade cumulus). In contrast to the model results of Koren et al. (2014), who suggested that warm invigoration saturates at higher aerosol loading (AOD ~ 0.3), our findings indicate a higher AOD of 0.41 (Figure 2), which is reasonable because the saturation value of AOD exhibits regional variability. For example, Kaufman et al. (2005) reported a maximum AOD of 0.46, while Zhang et al. (2021) found that the AOD in the ECS region is approximately 0.4. Considering the different processes associated with cloud regimes, we conducted the similar analysis for each cloud regime. Our findings reveal that the pattern of LWP adjustments is insensitive to cloud regime (Figure S5-S7), suggesting that they can be studied collectively.

Additionally, the observed LWP adjustments are results of meteorological covariations (Chen et al., 2014; Engström and Ekman, 2010; Zhang and Feingold, 2023). When we discuss ACI, the intricate interplay among meteorological factors, clouds and aerosols makes it difficult to exclude the influences from meteorological factors. Previous studies have employed various methods to exclude environmental confounding factors, such as opportunistic experiments from ship-track or volcano eruptions (Chen et al., 2022; Toll et al., 2019) where an overall weak LWP adjustment is observed. For satellite studies, Rosenfeld et al. (2019) pointed out that cloud thickness (H) explained almost three-fourths of meteorological impacts on cloud radiative effect (CRE) and they demonstrated an overall positive LWP adjustments when separating H. However, applying their method and constraining H in all intervals of Figure 1 (B and E), we find that LWP adjustments become negative, indicating that entrainment

processes dominate. The discrepancy may arise from their focus on samples in convective cores (top 10% of cloud optical thickness), which are closer to adiabatic, whereas our samples suggest more exchange with the free atmosphere.

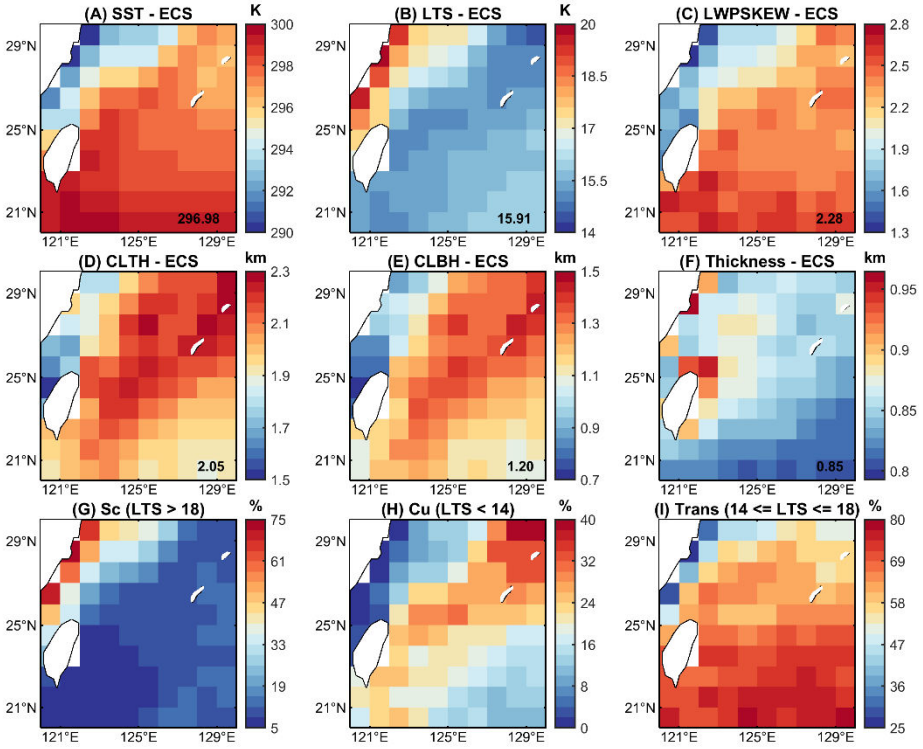

Figure 4. Distributions of meteorological factors and different cloud regimes in ECS region. (A) Sea Surface Temperature (SST) and (B) lower-tropospheric stability (LTS) are from ERA5 reanalysis data. (C) LWP skewness, (D) cloud-top height (CLTH), (E) cloud bottom height (CLBH) and (F) cloud thickness are directly or indirectly derived from SatCORPS Himawari-8 product. The numbers in the lower right corner represent regional averages being weighted by the cosine of latitude. Distribution of the proportion of cloud regimes for (G) Stratocumulus (Sc, LTS > 18 K), (H) Cumulus (Cu, LTS < 14 K), (I) Sc to Cu transition regime (Trans, 14 K <= LTS <= 18 K).

Fons et al. (2023) suggested H is an important confounder using causal approach and should be conditioned on. Here our results indicate the physical significance of constraining H. The sensitivity of LWP adjustments to H is clearly observed in Figure 1. In AUW region, negative LWP adjustments become weaker as H increases. This indicates that clouds of different H respond differently to entrainment. Thicker clouds with larger r_e are less sensitive to entrainment-feedback with increasing N_d compared to thinner clouds (Figure 1A). In other words, LWP in different H intervals responds differently to N_d so it is necessary to restrict H in order to exclude the effects of covariation. However,

in ECS region, negative LWP adjustments for clouds with H < 900 m become stronger with increasing H, while for clouds with H > 900 m, quite the contrary: it weakens with increasing H. The bidirectional sensitivity of LWP adjustments to H is likely attributed to distinct mixing characteristics among different cloud regimes in ECS region, reflecting the complex interactions between meteorological factors, clouds, and aerosols. Additionally, clouds above 800 m are associated with warm invigoration process (Figure 2). In this condition, H serves as a mediator but not a confounder. This implies that constraints on H in ECS is inappropriate because it fundamentally restricts a majority of mechanisms influencing cloud vertical development.

In summary, the above results reveal that LWP adjustments strongly depend on microphysical-dynamical processes (e.g. precipitation suppression, entrainment feedbacks and warm invigoration) and meteorological conditions (e.g. moisture and stability of the boundary layer). Given that some of these factors display diurnal variations in response to the solar radiation cycle, LWP adjustments would also exhibit diurnal patterns (black lines in Figure 1, C and F). We surmise that the prevailing dynamic conditions at any given time are responsible for the observed diurnal variations of LWP adjustments. To verify this hypothesis, we investigated the diurnal variations in LWP adjustments and their potential influencing factors.

3.2 How LWP adjustments change over diurnal scale and mechanisms

In AUW region, the negative LWP adjustments strengthen from around 0800 LT to 1300 LT, reaching the strongest at –0.41, and then weaken to –0.34. In ECS region, the positive LWP adjustments exhibit two local peaks during the observation period, occurring at 1200 LT and 1600 LT, with peak values of 0.07 and 0.21, respectively. Additionally, two local minima LWP adjustments are observed at 0800 LT and 1400 LT, with values of –0.11 and -0.06, respectively (Figure 1, C and F). The cloud-topped marine boundary layer (MBL) has been demonstrated to exhibit strong diurnal changes (Duynkerke and Hignett, 1993). Due to the observational limitations with passive satellite, it is not feasible to study the variations of MBL directly through its vertical profiles as with in-situ observations or active satellite (Albrecht et al., 1995; Luo et al., 2016). Instead, we can indirectly infer the boundary layer processes by examining the diurnal variations of cloud properties.

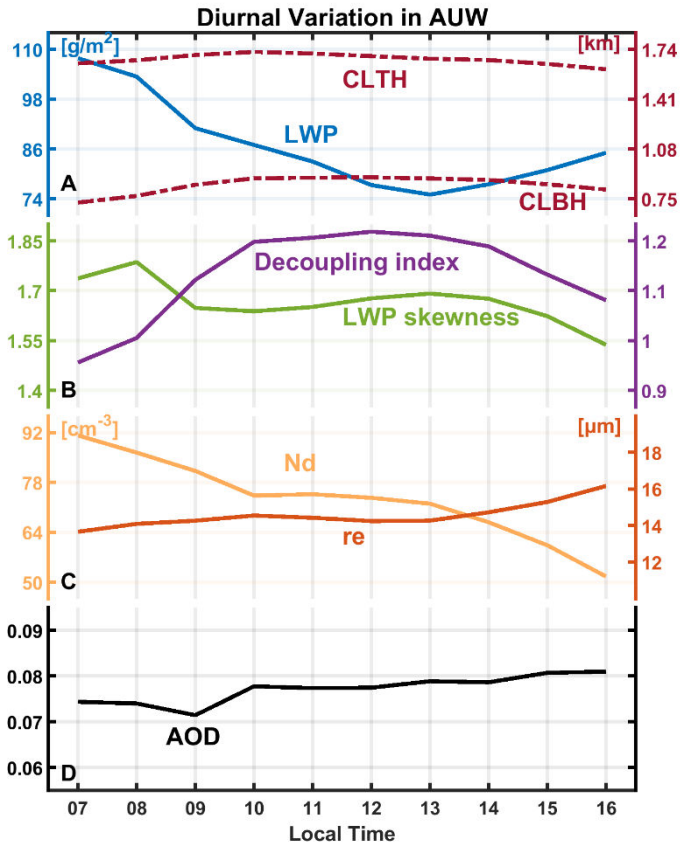

Figure 5. Diurnal patterns in AUW region. (A) Cloud liquid water path (LWP), cloud-top height (CLTH) and cloud bottom height (CLBH). (B) LWP skewness and decoupling index in AUW region. (C) Cloud droplet number concentration (N_d) and effective radius (r_e). (D) Aerosol optical depth (AOD).

AUW is one of the subtropical Sc regions over the eastern part of the ocean away from continent (Klein and Hartmann, 1993), characterized by large LTS and strong large-scale subsidence (Figure 3), which are conditions favorable for the formation of Sc. Figure 5 depicts the diurnal variations of cloud properties in the Sc-like AUW region. The diurnal variation of LWP shows a typical pattern with a peak in the morning and a gradual reduction until early afternoon. This pattern of variation is subject to diurnal cycle of solar insolation (Bretherton et al., 2004; Mechoso et al., 2014; Wood et al., 2002). Specifically, during daytime, solar radiation absorption within the cloud layer and long-wave cooling at cloud top drive the turbulent mixing within the cloud layer and inhibit turbulence to the sea surface, thus leading to the decoupling of MBL (Duynkerke and Hignett, 1993; Ghosh et al., 2005; Slingo et al., 1982). As decoupling cuts off the moisture source from the sea surface, the imbalance between entrainment drying and upward moisture flux may thin the cloud layer. The decrease of LWP before 1300 LT is primarily attributed to the lifting of cloud base which is in line with early modeling study for typical Sc cloud regimes (Bougeault, 1985), indicating that entrainment drying originates from evaporation at cloud base.

After 1300 LT, the gradual reduction of solar heating hinders the intensification of decoupling and helps rebuild the turbulence between the cloud and subcloud layer. Therefore, LWP increases after 1300 LT likely due to the reconstruction of turbulence.

Following the quantification method of Zheng et al. (2018) and Kazil et al. (2017), this study presents auxiliary verifications of decoupling process. First, according to Zheng et al. (2018), decoupling of the subtropical Sc decks during cold advection is often unstable (negative temperature advection). The formation of Cu beneath the Sc will render local coupling through feeding moisture into the upper cloud layer thus causing a positive skewness of probability density function (PDF) of LWP. Therefore, the skewness of LWP PDF can be used to estimate the degree of decoupling for each cloud sample:

$$\text{skewness} = \frac{\mathrm{E}(\mathrm{x}-\mathrm{u})^3}{\sigma^3} \tag{3}$$

where E is the expected value, μ and σ is the mean standard deviation of x, respectively. Positive skewness indicates more data tends to be distributed to the right, vice versa.

As shown in Figure 5, LWP skewness increases before 1300 LT and then decreases, illustrating the decoupling process and turbulence reconstruction discussed above. Note that while the cumulus penetration alters LWP, small variations in LWP skewness suggest that it cannot be directly compared with the reduction of LWP caused by decoupling, thus having no evident effect on the diurnal variation of LWP over AUW region. Additionally, due to the fluctuation of LWP skewness before 0900 LT, another decoupling index defined by Kazil et al. (2017) is used for further indication, quantifying the relative position between the CLBH and the lifting condensation level (LCL). A larger index implies a stronger degree of decoupling:

$$\text{decoupling index} = \frac{CLBH - LCL}{LCL} \tag{4}$$

The two indexes support each other and confirm the decoupling process.

Unexpectedly, there is no evident diurnal variation of AOD in AUW, but N_d continually declines from 0700 LT to 1600 LT and r_e does not change significantly before 1200 LT and then rises. It is thus reasonable to infer the diurnal variations of N_d and r_e are related with dynamic process on account of the disagreement with aerosols variations. Before 1200 LT, the decoupling that cuts off moisture transport suppresses condensational growth, while the shortwave heating counteracts longwave cooling, resulting in weakening of cloud-top entrainment (Verlinden, 2018.). The combination of these two processes leads to the little variation in r_e. Additionally, the continuous decrease in N_d before 1300 LT may be attributed

to the suppression of both surface moisture transport and cloud base updrafts (Stevens, 2000), which in turn reduce the supersaturation and hence the number of activated cloud droplets (Twomey, 1959). After 1200 LT, CLTH begins to decrease, according to $\frac{dCLTH}{dt} = w_s + w_e$ (Painemal et al., 2013), suggesting an intensification of large-scale subsidence (w_s, always negative in Sc region) and/or a weakening of entrainment rate (w_e). As large-scale subsidence becomes stronger, enhancing the temperature-inversion jump, which will in turn decrease the entrainment rate (Painemal et al., 2013). During this period, the condensational growth by the reconstructed water vapor supply will enhance r_e. Meanwhile, the coalescence process, enhanced by an increase in r_e leads to a decrease in N_d. This process could be more dominant than the increase in activated cloud droplets caused by water vapor reestablishment for an increase in N_d to be observed in this study.

Based on the diurnal mechanisms of MBL discussed above, the diurnal pattern of LWP adjustments is primarily a consequence of the influence of these diurnal-related mechanisms on the relationship between N_d and LWP across different microphysical-dynamical conditions. In AUW, the diurnal variations of the overall LWP adjustments (black line in Figure 1C) and LWP demonstrate a strong consistency with a turning point at 1300 LT. Since there is a single influence of increasing N_d on LWP in AUW region (i.e. the entrainment feedback), the variation of LWP adjustment here is mainly attributed to the gradual thinning of clouds, which reflects the differential LWP responses to N_d with varying H. LWP adjustment becomes more negative with the thinning of cloud, which is consistent with the results in Figure 1B.

In contrast, conditions of MBL in ECS region are more complicated. As mentioned in last section, ECS is a transition region due to "deepening-warming" process. Under this condition, MBL is never fully coupled but exhibits local cumulus coupling. Apparently, LWP skewness is a more appropriate indicator to reflect cumulus coupling in this region. Furthermore, the spatial distribution of LWP skewness can indicate the influence of cumulus coupling offshore (Figure 4C). For diurnal variations in ECS in Figure 6, there is a general decrease of LWP before 1300 LT followed by an increase. This is contrast to the pronounced cloud thinning observed in the AUW region due to the decoupling of MBL by solar heating. In the ECS region, the overall change of LWP is not significant (less than 10 g/m^2). Since MBL is never fully coupled, these minor observed changes are mainly caused by local cumulus coupling. The variations of LWP and LWP skewness exhibit a strong consistency. We also calculate the coefficient of variation

(c_v) of CLOT to represent the uniformity of each cloud sample. c_v is defined as the standard deviation (σ) divided by the mean(μ):

$$c_v = \frac{\sigma}{\mu} \tag{5}$$

The smaller the c_v is, the less dispersion there is among the cloud pixels in the cloud sample, resulting in a more uniform sample. It turns out that the cloud layer is influenced primarily by the strength of cumulus coupling, rather than other factors.

Diurnal variations of cumulus coupling can be also attributed to solar insolation. In the Sc to Cu transition region, the decoupled cloud layer and subcloud layer are often separated by a stable transition layer, which has been widely observed by the Atlantic Stratocumulus Transition Experiment (ASTEX) conducted over the northeast Atlantic Ocean. Based on ASTEX, Roger et al. (Rogers et al., 1995) suggested that the shortwave radiation would hinder convection during daytime by increasing the stability of the transition layer. Miller et al. (1998) extended this theory to the diurnal variations and believed that the diurnal variation of Cu development was regulated by the stability of the transition layer. Applying the theory to this area, the strongest stability of the transition layer occurs at 1300 LT due to absorption of solar radiation, at which point cumulus activity is the weakest. The earlier occurrence of the strongest stability in this study compared to the observations made during ASTEX may be attributed to the environment in the ECS region, which is more favorable for cumulus convection formation. This suggests that spontaneous convection is more likely to penetrate the transition layer in the ECS region.

In terms of microphysical properties, N_d in ECS decreases before 1100 LT and then increases. Variations of r_e are just the opposite except insignificant change since 1400 LT. The crucial mechanism leading to such changes may be attributed to the weakest entrainment drying at 1100 LT, resulting in the highest values of r_e and lowest values of N_d. And the change before 1100 LT may include the impacts of reducing AOD. Additionally, subsidence from both cloud top and bottom occurred after 1400 LT limits the entrainment and the continuous decline of r_e. But N_d continues to increase due to the effect of cumulus coupling after 1400 LT (Martin et al., 1995). Such diurnal variations in entrainment have also been observed in other coastal areas. Caldwell et al. (2005) reported the weakest entrainment rate at 1100 LT during East Pacific Investigation of Climate (EPIC) stratocumulus cruise in 2001. Painemal et al. (2017) found the minimum of entrainment occurred between 0900-1100 LT over the northeast Pacific region, attributing the diurnal pattern to the turbulence caused by long-wave radiative cooling.

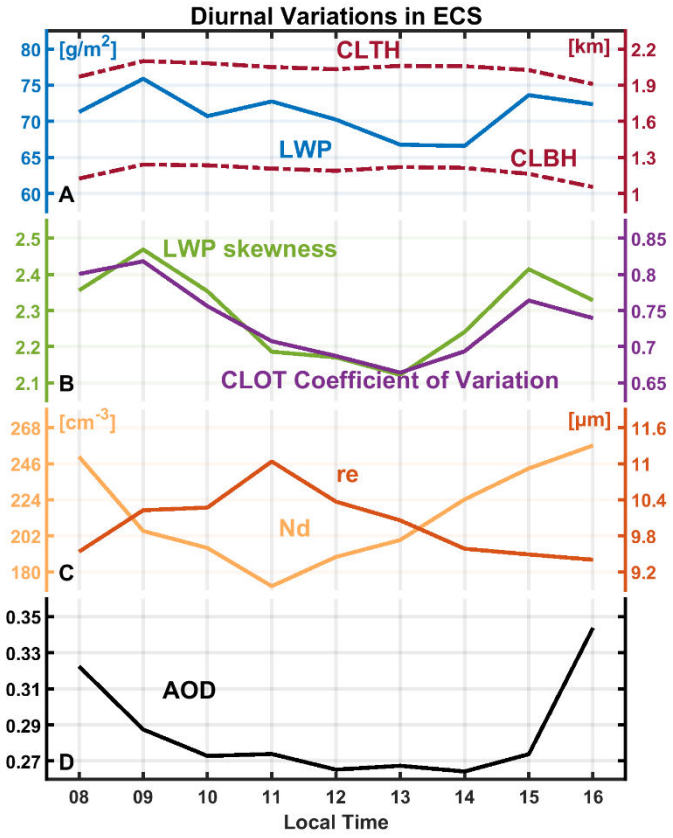

Figure 6. Diurnal patterns in ECS region. (A) Cloud liquid water path (LWP), cloud-top height (CLTH) and cloud bottom height (CLBH). (B) LWP skewness and coefficient of variation (c_v) of cloud optical depth (CLOT) in AUW region. (C) Cloud droplet number concentration (N_d) and effective radius (r_e). (D) Aerosol optical depth (AOD).

In the ECS region, the diurnal variation of LWP is relatively small, yet N_d exhibits a distinct diurnal pattern. Furthermore, the influence of N_d on LWP has two stages. As a result, changes in N_d lead to LWP adjustments that correspond to these two stages. Before 1100 LT, a decrease in N_d weakens the warm invigoration (blue line in Figure 1F), while the entrainment feedback intensifies (purple line in Figure 1F). After 1100 LT, the trend reverses. The interaction of these two processes drives the overall diurnal variation in LWP adjustments (black line in Figure 1F).

Figure 7 depicts schematics of the dominant mechanisms in the two regions. In AUW region, the primary mechanism behind diurnal variation of LWP adjustments is the cloud thinning driven by MBL decoupling before 1300 LT and the reconstruction of turbulence after 1300 LT. In ECS region, however, the H correlates with the intensity of cumulus coupling, while diurnal changes in entrainment dictate the diurnal variation of LWP adjustments. To summarize, the diurnal variations of LWP adjustments are primarily regulated by boundary layer dynamic processes. Failure to accurately capture these diurnal

variations in LWP adjustments and the underlying physical processes in observational studies may result in substantial inaccuracies in the quantification of regional and global LWP adjustments.

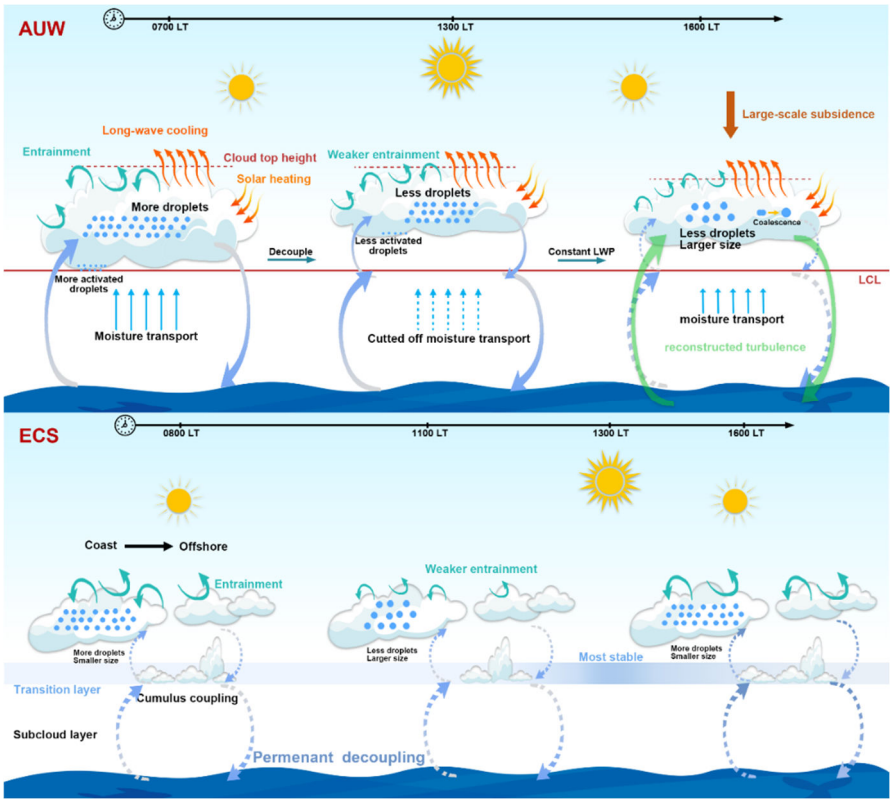

Figure 7. Schematics of diurnal dominant mechanisms observed in AUW and ECS regions. See text for details. Only the primary mechanisms are presented, while the relatively unimportant ones are omitted. Note that we represent the lifting condensation level (LCL) and transition layer at the same altitude for intuition. However, this depiction does not imply that their heights remain constant throughout the diurnal variation.

3.3 Impacts on aerosol indirect radiative effect if neglecting diurnal variations

Regional geostationary satellites observation reveals the significant impact of regional diurnal dynamic processes on LWP adjustments. LWP adjustments vary from –0.41 to –0.27 in AUW and from –0.11 to 0.21 in ECS. Diurnal averaged LWP adjustments are –0.31 and 0.02 considering the diurnal processes, respectively. The averaged LWP adjustment (dashed line in Figure 1, C and F) is not a simple average of the values, rather, it is derived from all available data within the region, accounting for diurnal covariation. This implies the inadequacy of previous observations only based on polar-orbiting satellites. For example, for Sc in AUW region, if LWP adjustments observed by polar-orbiting satellite (such as

MODIS overpass for aqua at 1330 LT or terra at 1030 LT) are applied to represent the whole day, the negative LWP adjustments will be obviously overestimated because the polar-orbiting observations failed to capture reconstruction of turbulence in the late afternoon. This bias will ultimately affect our estimation of cloud brightening in Twomey effect. The cloud albedo (A_c) susceptibility to aerosols can be estimated as Bellouin et al. (2020):

$$S = \frac{dA_C}{dN_d} = \frac{A_C(1 - A_C)}{3N_d}\left(1 + \frac{5}{2}\frac{d\ln LWP}{d\ln N_d}\right) \quad (6)$$

where S is the sensitivity of cloud albedo. According to this equation, LWP adjustments serve to regulate the cooling effect of the Twomey effect (the first term).

Following the method of (Glassmeier et al., 2021), we assume that climatological A_c is approximated as a constant value of the steady-state. Then the impact of LWP adjustments on S depends on $\left(1 + \frac{5}{2}\frac{d\ln LWP}{d\ln N_d}\right)$ according to Eq. 6. If we only consider LWP adjustments at fixed moments but neglect the diurnal variations, the cooling effect of LWP adjustments (strengthen Twomey effect) will be severely underestimated. For example, the average LWP adjustments at MODIS Aqua and Terra overpasses (1030 LT and 1330 LT) are −0.39 in AUW region and -0.04 in ECS region, respectively. The daily average LWP adjustments for the two regions are −0.31 and 0.02, respectively. After substituting these values into $\left(1 + \frac{5}{2}\frac{d\ln LWP}{d\ln N_d}\right)$, the cooling effect of LWP adjustments will be underestimated by |(0.225−0.025)/0.225|×100% = 89% in AUW region if neglecting the diurnal variations. This bias will lead to a further |(-0.39-(-0.31))/(−0.4)|×100% = 20% offset of the Twomey effect, as the Twomey effect is completely offset when the LWP adjustment is −0.4. Thereby the offset will steer aerosol indirect radiative effect towards a warming direction. Similarly, these two estimates are 14% and 15% for ECS region.

4 Discussion

Our analysis reveals the diurnal variations of LWP adjustments in two specific regions within the sight of Himawari-8, along with the possible mechanisms contributing to these variations. The observational studies demonstrate LWP adjustments in two regions are determined by the dominant microphysical-dynamical processes in different N_d stages, while their diurnal variations depend on dynamical conditions of boundary layer. In AUW region, diurnal variations are primarily associated with

the decoupling process of MBL, while in ECS region they are predominantly governed by the diurnal changes in cloud-top entrainment processes. LWP adjustments contribute to a broad range of uncertainties in the effective radiative forcing of ACI (ERF_{aci}) (IPCC, 2023). Here, we emphasize the time-dependent uncertainty observed by geostationary satellites, primarily stemming from varying dominant mechanisms at different times throughout the day. This is essentially a meteorological covariation on the daily time scale. We indicate an overall underestimation of cooling effect up to 89%, with a further 20% offset of the Twomey effect when neglecting the diurnal variations of LWP adjustments. Furthermore, our results quantify the impact of boundary layer feedback on LWP adjustments. For example, diurnal decoupling process in AUW region result in a 219% variation of LWP adjustments within the daytime relative to the daily mean (the diurnal variation range divided by daily mean), assuming other conditions remain relatively unchanged.

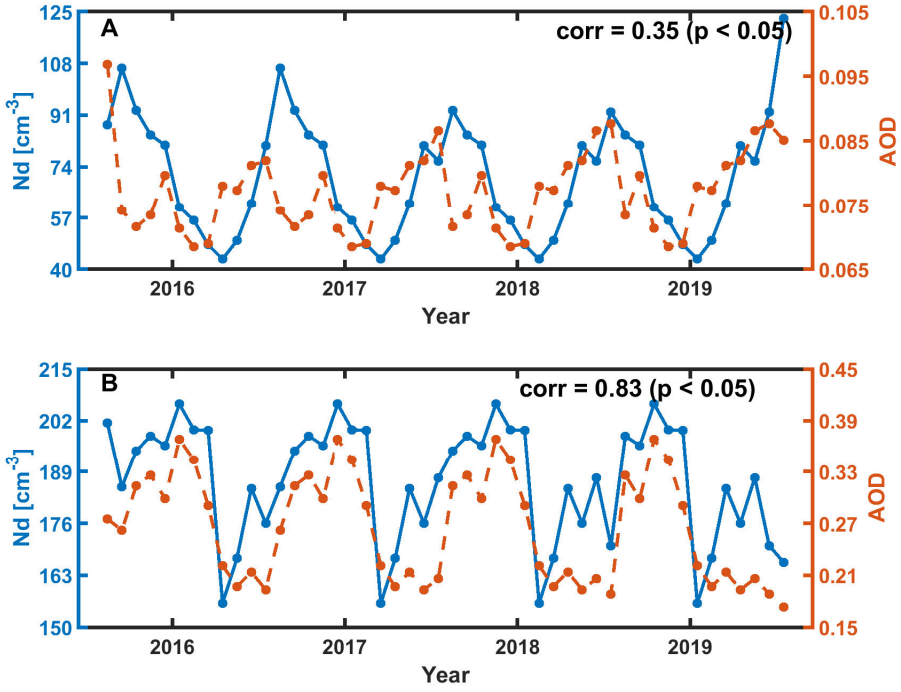

Figure 8. 4-year long-term variations of N_d and aerosol optical depth (AOD) from MERRA-2 at 1200 LT in AUW (A) and ECS (B) region. The correlation coefficients (corr) between N_d and AOD are 0.35 and 0.83 (significant at the 95% confidence level), respectively.

It is worth noting that our results also reveal diurnal variations of N_d, a core indicator in ACI, which are also attributed to the MBL diurnal processes. While previous studies have analyzed the long-term variations of N_d, highlighting the key role of aerosols (Hu et al., 2021; Li et al., 2018; McCoy et al., 2015,

2018; Quaas et al., 2006), unexpectedly, there is no good consistency between them in diurnal variations. This discrepancy may stem from previous polar-orbiting satellite observations at fixed times have overlooked the crucial role played by other physical mechanisms at different times. In fact, geostationary satellite assessments (Figure 8) uncover significant correlations observed between the 4-year long-term variations of AOD and N_d at 1200 LT in both regions, particularly in ECS with a correlation of 0.83. Meanwhile, both regions show the similar distribution patterns, with higher N_d and smaller r_e near the continental coastal area, aligning with the average AOD spatial distribution (spatial correlation coefficients of 0.78 in AUW and 0.84 in ECS) (Figure S1), suggesting a pronounced impact of anthropogenic activities on cloud microphysical properties on a long-term scale. Note that the correlations between AOD and N_d at certain fixed times are not statistically significant (not shown). This may be due to the relatively insignificant impact of aerosol effects at these moments, while other physical processes may exert a more pronounced influence. Future researches should broaden its scope to investigate effects of other physical processes on N_d at specific times, in addition to the roles of aerosols. Moreover, in the context of global warming, whether these physical processes will be affected and consequently contribute to variations of N_d deserves further investigation.

Several limitations should be acknowledged in this study. First, the time-dependence of LWP adjustments we discussed differs from the cloud evolution process, emphasizing diurnal variations caused by changes in dominant mechanisms at different times rather than tracking the evolution of individual clouds. This approach may introduce uncertainties into our results since the full cloud life cycle and evolution is not the same with diurnal variations. The full cloud lifetime evolution associated with LWP adjustments is not the scope of this study and warrant further exploration. Additionally, given the scarcity of observational data at fine scales, certain mechanisms are indirectly inferred from observational index (e.g., decoupling process inferred from LWP skewness), which needs further microphysical-process based in-situ observations as well as model simulations. Finally, uncertainties of retrievals have been discussed in Data and Methods, which provides further context for the limitations of our study.

In summary, our research provides a novel perspective for investigating the diurnal variation of LWP adjustments, focusing on how microphysical-dynamical processes in clouds are influenced by the diurnal variations of the boundary layer processes. We underscore the importance of fully considering the covariation with environmental conditions, indicating different potential influencing factors on cloud

brightening and radiative forcing in terms of the regional and diurnal daytime scale.

References

Ackerman, A. S., Kirkpatrick, M. P., Stevens, D. E., and Toon, O. B.: The impact of humidity above stratiform clouds on indirect aerosol climate forcing, Nature, 432, 1014–1017, https://doi.org/10.1038/nature03174, 2004.

Albrecht, B. A., Bretherton, C. S., Johnson, D., Scubert, W. H., and Frisch, A. S.: The Atlantic Stratocumulus Transition Experiment—ASTEX, Bulletin of the American Meteorological Society, 76, 889–904, https://doi.org/10.1175/1520-0477(1995)076<0889:TASTE>2.0.CO;2, 1995.

Altaratz, O., Koren, I., Remer, L. A., and Hirsch, E.: Review: Cloud invigoration by aerosols—Coupling between microphysics and dynamics, Atmospheric Research, 140–141, 38–60, https://doi.org/10.1016/j.atmosres.2014.01.009, 2014.

Bellouin, N., Quaas, J., Gryspeerdt, E., Kinne, S., Stier, P., Watson-Parris, D., Boucher, O., Carslaw, K. S., Christensen, M., Daniau, A. -L., Dufresne, J. -L., Feingold, G., Fiedler, S., Forster, P., Gettelman, A., Haywood, J. M., Lohmann, U., Malavelle, F., Mauritsen, T., McCoy, D. T., Myhre, G., Mülmenstädt, J., Neubauer, D., Possner, A., Rugenstein, M., Sato, Y., Schulz, M., Schwartz, S. E., Sourdeval, O., Storelvmo, T., Toll, V., Winker, D., and Stevens, B.: Bounding Global Aerosol Radiative Forcing of Climate Change, Rev. Geophys., 58, https://doi.org/10.1029/2019RG000660, 2020.

Bender, F. A.-M., Frey, L., McCoy, D. T., Grosvenor, D. P., and Mohrmann, J. K.: Assessment of aerosol–cloud–radiation correlations in satellite observations, climate models and reanalysis, Clim Dyn, 52, 4371–4392, https://doi.org/10.1007/s00382-018-4384-z, 2019.

Bennartz, R.: Global assessment of marine boundary layer cloud droplet number concentration from satellite, J. Geophys. Res., 112, D02201, https://doi.org/10.1029/2006JD007547, 2007.

Bougeault, P.: The Diurnal Cycle of the Marine Stratocumulus Layer: A Higher-Order Model Study, Journal of the Atmospheric Sciences, 42, 2826–2843, https://doi.org/10.1175/1520-0469(1985)042<2826:TDCOTM>2.0.CO;2, 1985.

Bretherton, C. S. and Wyant, M. C.: Moisture Transport, Lower-Tropospheric Stability, and Decoupling of Cloud-Topped Boundary Layers, Journal of the Atmospheric Sciences, 54, 148–167, https://doi.org/10.1175/1520-0469(1997)054<0148:MTLTSA>2.0.CO;2, 1997.

Bretherton, C. S., Uttal, T., Fairall, C. W., Yuter, S. E., Weller, R. A., Baumgardner, D., Comstock, K., Wood, R., and Raga, G. B.: The Epic 2001 Stratocumulus Study, Bulletin of the American Meteorological Society, 85, 967–978, https://doi.org/10.1175/BAMS-85-7-967, 2004.

Caldwell, P., Bretherton, C. S., and Wood, R.: Mixed-Layer Budget Analysis of the Diurnal Cycle of Entrainment in Southeast Pacific Stratocumulus, Journal of the Atmospheric Sciences, 62, 3775–3791, https://doi.org/10.1175/JAS3561.1, 2005.

Change (IPCC), I. P. on C.: The Earth's Energy Budget, Climate Feedbacks and Climate Sensitivity, in: Climate Change 2021 – The Physical Science Basis: Working Group I Contribution to the Sixth Assessment Report of the Intergovernmental Panel on Climate Change, Cambridge University Press, 923–1054, 2023.

Chen, Y., Haywood, J., Wang, Y., Malavelle, F., Jordan, G., Partridge, D., Fieldsend, J., De Leeuw, J., Schmidt, A., Cho, N., Oreopoulos, L., Platnick, S., Grosvenor, D., Field, P., and Lohmann, U.: Machine learning reveals climate forcing from aerosols is dominated by increased cloud cover, Nat. Geosci., 15, 609–614, https://doi.org/10.1038/s41561-022-00991-6, 2022.

Chen, Y.-C., Christensen, M. W., Stephens, G. L., and Seinfeld, J. H.: Satellite-based estimate of global aerosol–cloud radiative forcing by marine warm clouds, Nature Geosci, 7, 643–646, https://doi.org/10.1038/ngeo2214, 2014.

Duynkerke, P. G. and Hignett, P.: Simulation of Diurnal Variation in a Stratocumulus-capped Marine Boundary Layer during FIRE, Monthly Weather Review, 121, 3291–3300, https://doi.org/10.1175/1520-0493(1993)121<3291:SODVIA>2.0.CO;2, 1993.

Engström, A. and Ekman, A. M. L.: Impact of meteorological factors on the correlation between aerosol optical depth and cloud fraction: IMPACTS ON AEROSOL-CLOUD RELATIONSHIPS, Geophys. Res. Lett., 37, n/a-n/a, https://doi.org/10.1029/2010GL044361, 2010.

Fons, E., Runge, J., Neubauer, D., and Lohmann, U.: Stratocumulus adjustments to aerosol perturbations disentangled with a causal approach, npj Clim Atmos Sci, 6, 130, https://doi.org/10.1038/s41612-023-00452-w, 2023.

Ghosh, S., Osborne, S., and Smith, M. H.: On the importance of cumulus penetration on the microphysical and optical properties of stratocumulus clouds, Atmospheric Chemistry and Physics, 5, 755–765, https://doi.org/10.5194/acp-5-755-2005, 2005.

Glassmeier, F., Hoffmann, F., Johnson, J. S., Yamaguchi, T., Carslaw, K. S., and Feingold, G.: Aerosol-cloud-climate cooling overestimated by ship-track data, Science, 371, 485–489, https://doi.org/10.1126/science.abd3980, 2021.

Grosvenor, D. P., Sourdeval, O., Zuidema, P., Ackerman, A., Alexandrov, M. D., Bennartz, R., Boers, R., Cairns, B., Chiu, J. C., Christensen, M., Deneke, H., Diamond, M., Feingold, G., Fridlind, A., Hünerbein, A., Knist, C., Kollias, P., Marshak, A., McCoy, D., Merk, D., Painemal, D., Rausch, J., Rosenfeld, D., Russchenberg, H., Seifert, P., Sinclair, K., Stier, P., van Diedenhoven, B., Wendisch, M., Werner, F., Wood, R., Zhang, Z., and Quaas, J.: Remote Sensing of Droplet Number Concentration in Warm Clouds: A Review of the Current State of Knowledge and Perspectives, Reviews of Geophysics, 56, 409–453, https://doi.org/10.1029/2017RG000593, 2018.

Gryspeerdt, E., Goren, T., Sourdeval, O., Quaas, J., Mülmenstädt, J., Dipu, S., Unglaub, C., Gettelman, A., and Christensen, M.: Constraining the aerosol influence on cloud liquid water path, Atmos. Chem. Phys., 19, 5331–5347, https://doi.org/10.5194/acp-19-5331-2019, 2019.

Hu, Y., Lu, X., Zhai, P.-W., Hostetler, C. A., Hair, J. W., Cairns, B., Sun, W., Stamnes, S., Omar, A., Baize, R., Videen, G., Mace, J., McCoy, D. T., McCoy, I. L., and Wood, R.: Liquid Phase Cloud Microphysical Property Estimates From CALIPSO Measurements, Front. Remote Sens., 2, https://doi.org/10.3389/frsen.2021.724615, 2021.

Kang, L., Marchand, R., and Smith, W.: Evaluation of MODIS and Himawari-8 Low Clouds Retrievals Over the Southern Ocean With In Situ Measurements From the SOCRATES Campaign, Earth and Space Science, 8, https://doi.org/10.1029/2020EA001397, 2021.

Kaufman, Y. J., Koren, I., Remer, L. A., Rosenfeld, D., and Rudich, Y.: The effect of smoke, dust, and pollution aerosol on shallow cloud development over the Atlantic Ocean, Proc. Natl. Acad. Sci. U.S.A., 102, 11207–11212, https://doi.org/10.1073/pnas.0505191102, 2005.

Kazil, J., Yamaguchi, T., and Feingold, G.: Mesoscale organization, entrainment, and the properties of a closed-cell stratocumulus cloud, Journal of Advances in Modeling Earth Systems, 9, 2214–2229, https://doi.org/10.1002/2017MS001072, 2017.

Klein, S. A. and Hartmann, D. L.: The Seasonal Cycle of Low Stratiform Clouds, Journal of Climate, 6, 1587–1606, https://doi.org/10.1175/1520-0442(1993)006<1587:TSCOLS>2.0.CO;2, 1993.

Koren, I., Dagan, G., and Altaratz, O.: From aerosol-limited to invigoration of warm convective clouds,

Science, 344, 1143–1146, https://doi.org/10.1126/science.1252595, 2014.

Lee, S. S., Penner, J. E., and Saleeby, S. M.: Aerosol effects on liquid-water path of thin stratocumulus clouds, J. Geophys. Res., 114, D07204, https://doi.org/10.1029/2008JD010513, 2009.

Li, J., Jian, B., Huang, J., Hu, Y., Zhao, C., Kawamoto, K., Liao, S., and Wu, M.: Long-term variation of cloud droplet number concentrations from space-based Lidar, Remote Sensing of Environment, 213, 144–161, https://doi.org/10.1016/j.rse.2018.05.011, 2018.

Luo, T., Wang, Z., Zhang, D., and Chen, B.: Marine boundary layer structure as observed by A-train satellites, Atmospheric Chemistry and Physics, 16, 5891–5903, https://doi.org/10.5194/acp-16-5891-2016, 2016.

Martin, G. M., Johnson, D. W., Rogers, D. P., Jonas, P. R., Minnis, P., and Hegg, D. A.: Observations of the Interaction between Cumulus Clouds and Warm Stratocumulus Clouds in the Marine Boundary Layer during ASTEX, Journal of the Atmospheric Sciences, 52, 2902–2922, https://doi.org/10.1175/1520-0469(1995)052<2902:OOTIBC>2.0.CO;2, 1995.

McCoy, D. T., Burrows, S. M., Wood, R., Grosvenor, D. P., Elliott, S. M., Ma, P.-L., Rasch, P. J., and Hartmann, D. L.: Natural aerosols explain seasonal and spatial patterns of Southern Ocean cloud albedo, Sci. Adv., 1, e1500157, https://doi.org/10.1126/sciadv.1500157, 2015.

McCoy, D. T., Bender, F. A.-M., Grosvenor, D. P., Mohrmann, J. K., Hartmann, D. L., Wood, R., and Field, P. R.: Predicting decadal trends in cloud droplet number concentration using reanalysis and satellite data, Atmos. Chem. Phys., 18, 2035–2047, https://doi.org/10.5194/acp-18-2035-2018, 2018.

Mechoso, C. R., Wood, R., Weller, R., Bretherton, C. S., Clarke, A. D., Coe, H., Fairall, C., Farrar, J. T., Feingold, G., Garreaud, R., Grados, C., McWilliams, J., Szoeke, S. P. de, Yuter, S. E., and Zuidema, P.: Ocean–Cloud–Atmosphere–Land Interactions in the Southeastern Pacific: The VOCALS Program, Bulletin of the American Meteorological Society, 95, 357–375, https://doi.org/10.1175/BAMS-D-11-00246.1, 2014.

Michibata, T., Suzuki, K., Sato, Y., and Takemura, T.: The source of discrepancies in aerosol–cloud–precipitation interactions between GCM and A-Train retrievals, Atmos. Chem. Phys., 16, 15413–15424, https://doi.org/10.5194/acp-16-15413-2016, 2016.

Miller, M. A., Jensen, M. P., and Clothiaux, E. E.: Diurnal Cloud and Thermodynamic Variations in the Stratocumulus Transition Regime: A Case Study Using In Situ and Remote Sensors, Journal of the Atmospheric Sciences, 55, 2294–2310, https://doi.org/10.1175/1520-0469(1998)055<2294:DCATVI>2.0.CO;2, 1998.

Miller, S. D., Rogers, M. A., Haynes, J. M., Sengupta, M., and Heidinger, A. K.: Short-term solar irradiance forecasting via satellite/model coupling, Solar Energy, 168, 102–117, https://doi.org/10.1016/j.solener.2017.11.049, 2018.

Painemal, D., Minnis, P., and O'Neill, L.: The Diurnal Cycle of Cloud-Top Height and Cloud Cover over the Southeastern Pacific as Observed by GOES-10, Journal of the Atmospheric Sciences, 70, 2393–2408, https://doi.org/10.1175/JAS-D-12-0325.1, 2013.

Painemal, D., Xu, K., Palikonda, R., and Minnis, P.: Entrainment rate diurnal cycle in marine stratiform clouds estimated from geostationary satellite retrievals and a meteorological forecast model, Geophysical Research Letters, 44, 7482–7489, https://doi.org/10.1002/2017GL074481, 2017.

Possner, A., Eastman, R., Bender, F., and Glassmeier, F.: Deconvolution of boundary layer depth and aerosol constraints on cloud water path in subtropical stratocumulus decks, Atmos. Chem. Phys., 20, 3609–3621, https://doi.org/10.5194/acp-20-3609-2020, 2020.

Qiu, S., Zheng, X., Painemal, D., Terai, C. R., and Zhou, X.: Daytime variation in the aerosol indirect

effect for warm marine boundary layer clouds in the eastern North Atlantic, Atmospheric Chemistry and Physics, 24, 2913–2935, https://doi.org/10.5194/acp-24-2913-2024, 2024.

Quaas, J., Boucher, O., and Lohmann, U.: Constraining the total aerosol indirect effect in the LMDZ and ECHAM4 GCMs using MODIS satellite data, Atmospheric Chemistry and Physics, 6, 947–955, https://doi.org/10.5194/acp-6-947-2006, 2006.

Rogers, D. P., Yang, X., Norris, P. M., Johnson, D. W., Martin, G. M., Friehe, C. A., and Berger, B. W.: Diurnal Evolution of the Cloud-Topped Marine Boundary Layer. Part I: Nocturnal Stratocumulus Development, Journal of the Atmospheric Sciences, 52, 2953–2966, https://doi.org/10.1175/1520-0469(1995)052<2953:DEOTCT>2.0.CO;2, 1995.

Rosenfeld, D., Wang, H., and Rasch, P. J.: The roles of cloud drop effective radius and LWP in determining rain properties in marine stratocumulus, Geophysical Research Letters, 39, https://doi.org/10.1029/2012GL052028, 2012.

Rosenfeld, D., Zhu, Y., Wang, M., Zheng, Y., Goren, T., and Yu, S.: Aerosol-driven droplet concentrations dominate coverage and water of oceanic low-level clouds, Science, 363, eaav0566, https://doi.org/10.1126/science.aav0566, 2019.

Slingo, A., Nicholls, S., and Schmetz, J.: Aircraft observations of marine stratocumulus during JASIN, Quart J Royal Meteoro Soc, 108, 833–856, https://doi.org/10.1002/qj.49710845807, 1982.

Small, J. D., Chuang, P. Y., Feingold, G., and Jiang, H.: Can aerosol decrease cloud lifetime?, Geophys. Res. Lett., 36, L16806, https://doi.org/10.1029/2009GL038888, 2009.

Stevens, B.: Cloud transitions and decoupling in shear - free stratocumulus - topped boundary layers, Geophysical Research Letters, 27, 2557–2560, https://doi.org/10.1029/1999GL011257, 2000.

Toll, V., Christensen, M., Quaas, J., and Bellouin, N.: Weak average liquid-cloud-water response to anthropogenic aerosols, Nature, 572, 51–55, https://doi.org/10.1038/s41586-019-1423-9, 2019.

Trepte, Q. Z., Minnis, P., Sun-Mack, S., Yost, C. R., Chen, Y., Jin, Z., Hong, G., Chang, F.-L., Smith, W. L., Bedka, K. M., and Chee, T. L.: Global Cloud Detection for CERES Edition 4 Using Terra and Aqua MODIS Data, IEEE Transactions on Geoscience and Remote Sensing, 57, 9410–9449, https://doi.org/10.1109/TGRS.2019.2926620, 2019.

Twomey, S.: The nuclei of natural cloud formation part II: The supersaturation in natural clouds and the variation of cloud droplet concentration, Geofisica Pura e Applicata, 43, 243–249, https://doi.org/10.1007/BF01993560, 1959.

Marine Low Clouds : Radiation, Turbulence, and Forecasting:

Wood, R., Bretherton, C. S., and Hartmann, D. L.: Diurnal cycle of liquid water path over the subtropical and tropical oceans: DIURNAL CYCLE OF LIQUID WATER PATH, Geophys. Res. Lett., 29, 7-1-7–4, https://doi.org/10.1029/2002GL015371, 2002.

Yost, C. R., Minnis, P., Sun-Mack, S., Chen, Y., and Smith, W. L.: CERES MODIS Cloud Product Retrievals for Edition 4—Part II: Comparisons to CloudSat and CALIPSO, IEEE Transactions on Geoscience and Remote Sensing, 59, 3695–3724, https://doi.org/10.1109/TGRS.2020.3015155, 2021.

Zhang, J. and Feingold, G.: Distinct regional meteorological influences on low-cloud albedo susceptibility over global marine stratocumulus regions, Atmospheric Chemistry and Physics, 23, 1073–1090, https://doi.org/10.5194/acp-23-1073-2023, 2023.

Zhang, X., Wang, H., Che, H.-Z., Tan, S.-C., Yao, X.-P., Peng, Y., and Shi, G.-Y.: Radiative forcing of the aerosol-cloud interaction in seriously polluted East China and East China Sea, Atmospheric Research, 252, 105405, https://doi.org/10.1016/j.atmosres.2020.105405, 2021.

Zheng, Y., Rosenfeld, D., and Li, Z.: Estimating the Decoupling Degree of Subtropical Marine

Stratocumulus Decks From Satellite, Geophysical Research Letters, 45, 12,560-12,568, https://doi.org/10.1029/2018GL078382, 2018.

630

Supplementary Materials

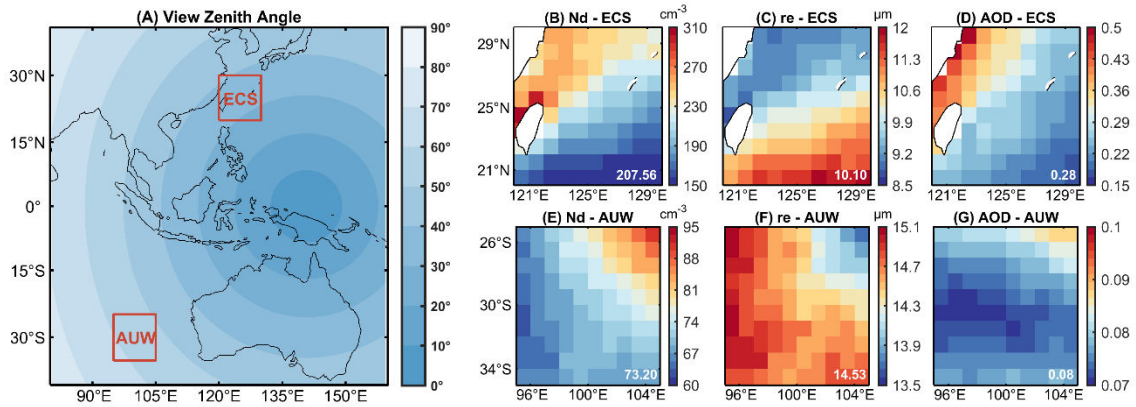

Figure S1. Distributions of cloud properties in two typical regions (the east China sea (20º-30ºN, 120º-130ºE, ECS) and the west of Australia (25º-35ºS, 95º-105ºE, AUW). (A) Geographical

635 distribution of the view zenith angle of Satellite Cloud and Radiation Property retrieval System (SatCORPS) Himawari-8 data. The selected regions are marked by red boxes. Spatial distributions of cloud droplet number concentration (N_d) (B, E), effective radius (r_e) (C, F) and aerosol optical depth (AOD) (D, G) from MERRA-2 data are presented. The numbers in the lower right corner represent regional averages being weighted by the cosine of latitude.

640

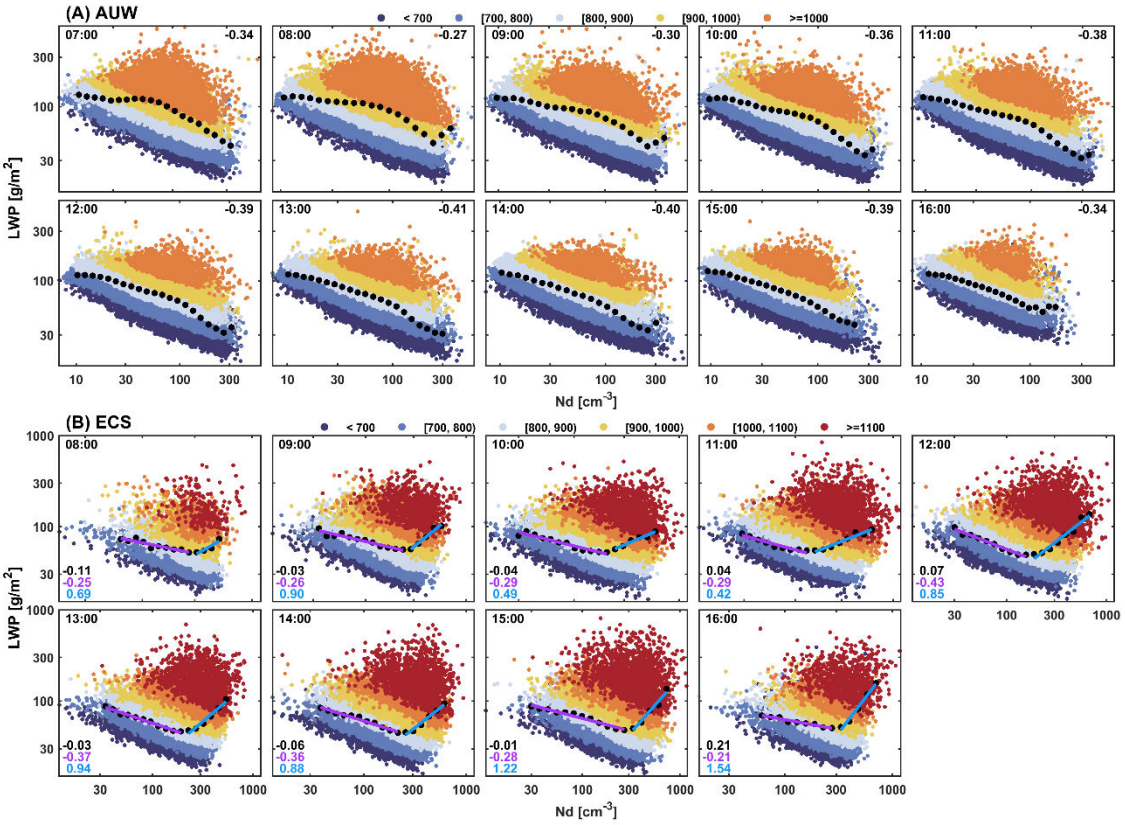

Figure S2. The complete diurnal pictures of LWP adjustments in AUW (A) and ECS (B) region. Colored dots are samples in different cloud thickness (H) bins (unit: m). Black dots represent median LWP in each N_d bin. The colored lines are the fits of black dots at different Nd stages, with values showed in corresponding color. The black number means the fitted value of all the black dots. Stages in (B) represented by purple lines are the stages dominated by the entrainment process. Blue line is another stage when the cloud invigoration effect by condensation exceeds the cloud suppression effect by entrainment. The fitted value for each stage is labeled with corresponding colors.

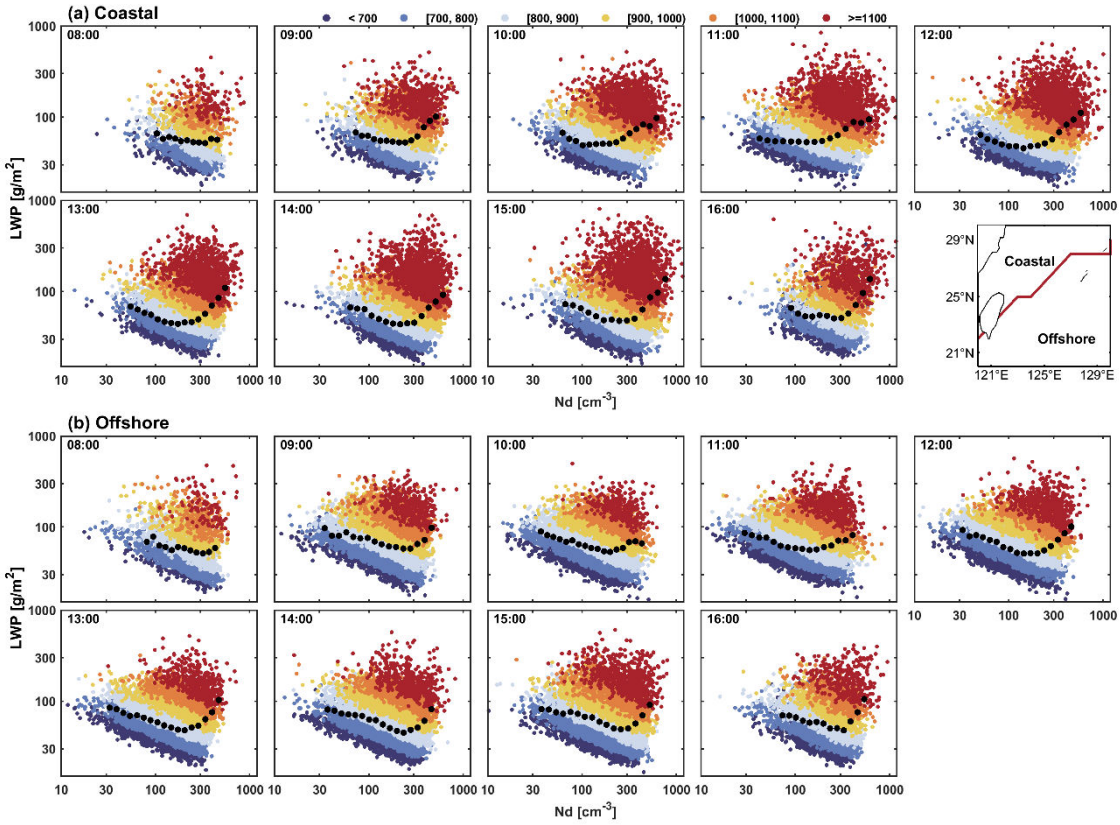

650

Figure S3. The complete diurnal pictures of LWP adjustments in coastal (A) and offshore (B) areas. The boundary of two areas are divided by the distribution of N_d in Figure S1. The coastal area is the area with 4-year averaged N_d lager than 220 cm^{-3} and the offshore area is the area with 4-year averaged N_d less than 220 cm^{-3}.

655

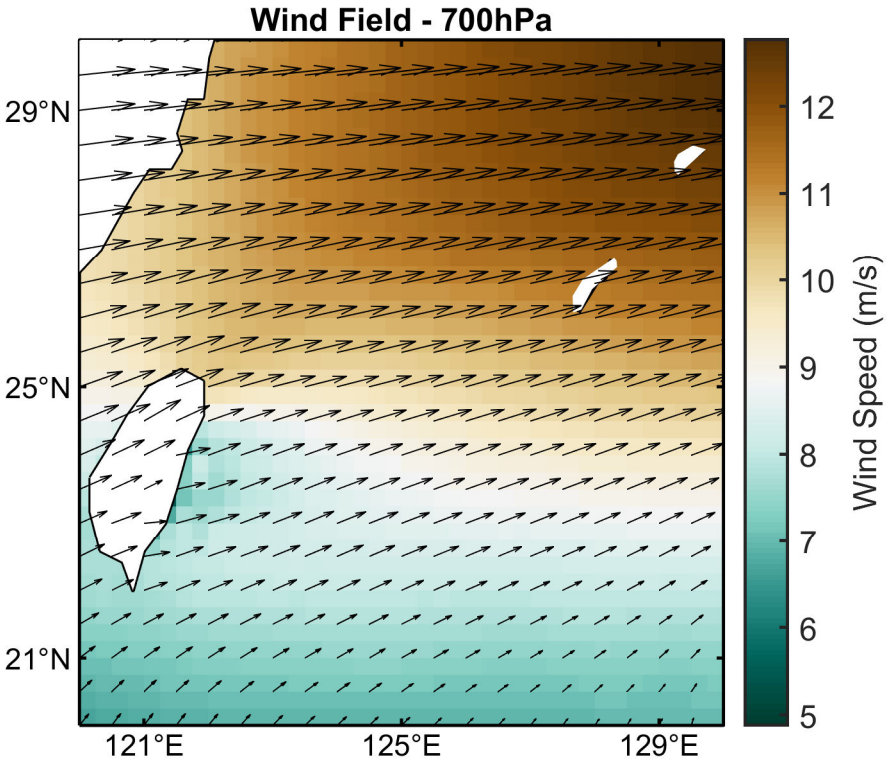

Figure S4. Horizontal wind field at 700 hPa in ECS region.

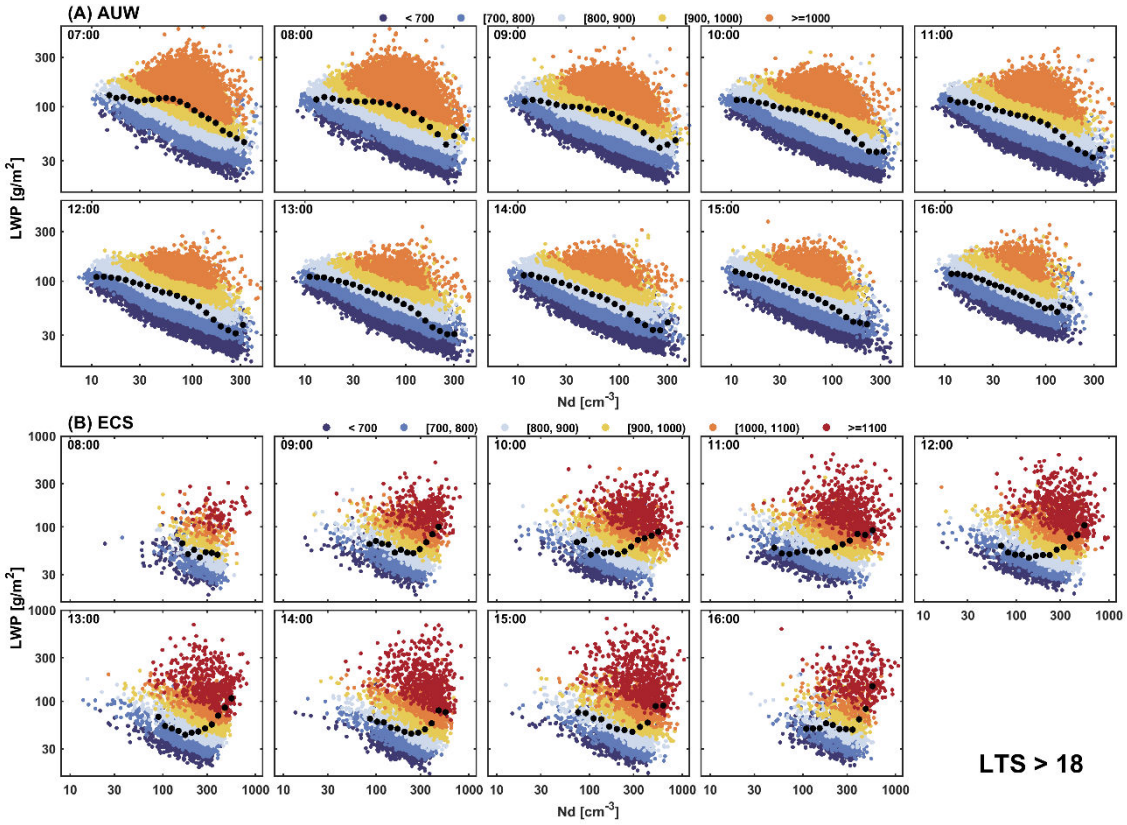

660

Figure S5. The complete diurnal pictures of LWP adjustments in AUW (A) and ECS (B) region with the samples of Sc clouds (LTS > 18 K).

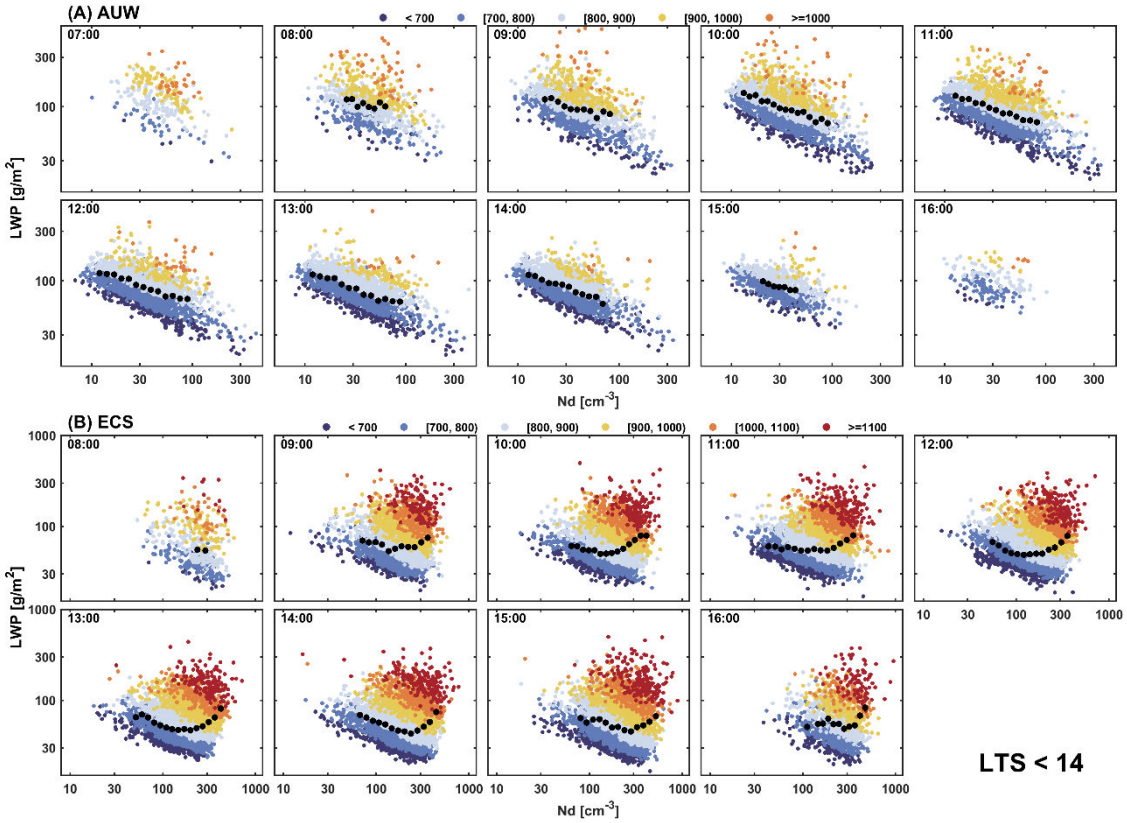

665 **Figure S6. The complete diurnal pictures of LWP adjustments in AUW (A) and ECS (B) region with the samples of Cu clouds (LTS < 14 K).**

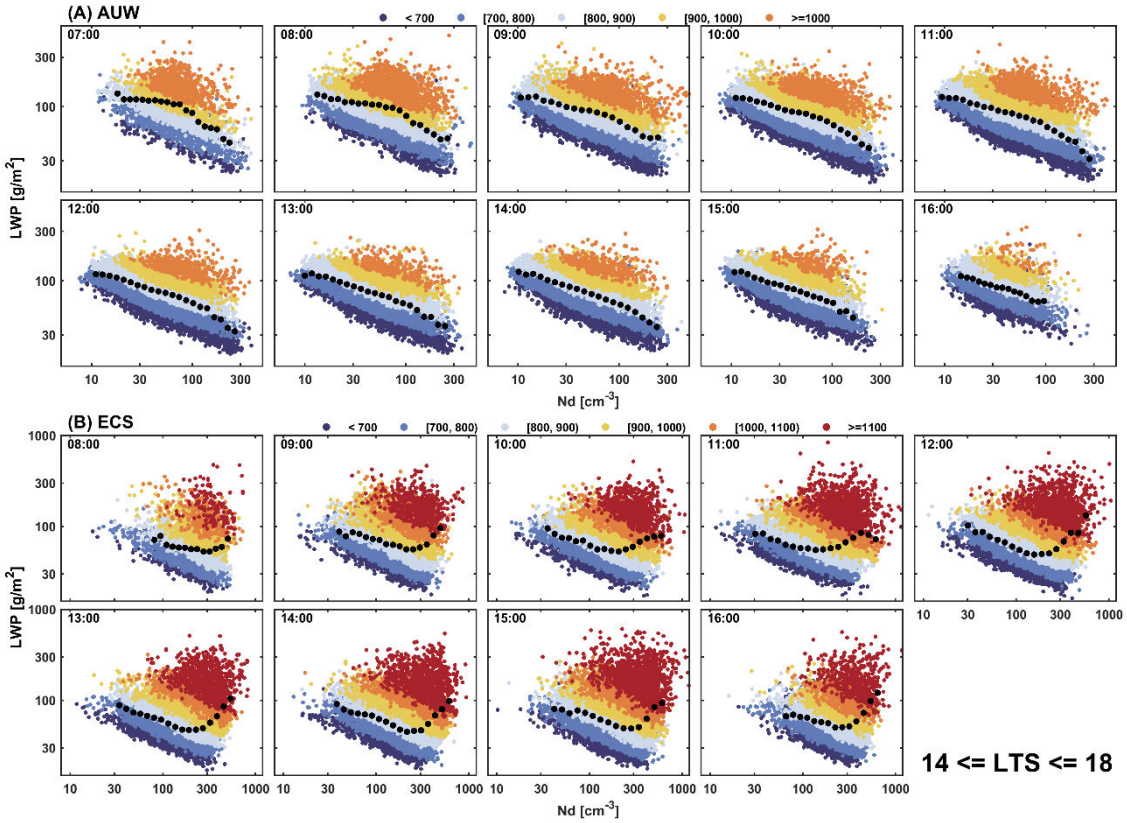

Figure S7. The complete diurnal pictures of LWP adjustments in AUW (A) and ECS (B) region with the samples of Sc to Cu transition regime (14 K <= LTS <= 18 K).